J. Harbison/ED

# COMPUTATIONAL FLUID MECHANICS UTILIZING THE VARIATIONAL PRINCIPLE OF MODELING DAMPING SEALS

Final Report, Contract No. NAS8-35508

CI-FR-0088



Prepared for:

National Aeronautics and Space Administration
George C. Marshall Space Flight Center
Marshall Space Flight Center, AL 35812

By:

J. Michael Abernathy

**CONTINUUM, Inc.**
4715 University Drive, Suite 118
Huntsville, AL 35816-3495

# COMPUTATIONAL FLUID MECHANICS UTILIZING THE VARIATIONAL PRINCIPLE OF MODELING DAMPING SEALS

Final Report, Contract No. NAS8-35508

CI-FR-0088

Prepared for:

National Aeronautics and Space Administration
George C. Marshall Space Flight Center
Marshall Space Flight Center, AL 35812

By:

J. Michael Abernathy

**CONTINUUM, Inc.**
4715 University Drive, Suite 118
Huntsville, AL 35816-3495

May 1, 1986

## SUMMARY

A computational fluid dynamics code for application to traditional incompressible flow problems has been developed. The method is actually a slight compressibility approach which takes advantage of the bulk modulus and finite sound speed of all real fluids. The finite element numerical analog uses a dynamic differencing scheme based, in part, on a variational principle for computational fluid dynamics. The code was developed in order to study the feasibility of damping seals for high speed turbomachinery. Preliminary seal analyses have been performed.

This report was prepared by Continuum, Inc. for NASA-MSFC under contract NAS8-35508.

## TABLE OF CONTENTS

Summary ..... i
Table of Contents ..... ii
Table of Figures ..... iii
Nomenclature ..... iv
Introduction ..... 1
Treatment of the Velocity-Pressure Coupling ..... 3
Theory ..... 6
  Basic Equations ..... 6
  Pressure Solution ..... 7
  Numerical Analog ..... 8
  Turbulence Model ..... 10
Results ..... 13
  Vectorization ..... 13
  Rotating Cylinders ..... 13
  Three-Dimensional Results ..... 20
  Computational Requirements ..... 25
Conclusions ..... 27
References ..... 28

## TABLE OF FIGURES

Fig. 1 Couette Flow Velocities for Air . . . . . 14

Fig. 2 Couette Flow Velocities for Water . . . . . 15

Fig. 3 Radial Velocity Profile for Rotating Cylinders . . . . . 17

Fig. 4 Pressures for Cylinders with Air from Compressible VAST Code . . . . . 18

Fig. 5 Radial Pressure Profile for Rotating Cylinders with Water . . . . . 19

Fig. 6 Grid and Element Detail for Damping Seal Model . . . . . 21

Fig. 7 Rotor Velocities in the Seal . . . . . 22

Fig. 8 Cross-Section of Velocities in the Seal . . . . . 23

Fig. 9 Cross-Section of Pressures in the Seal . . . . . 24

## NOMENCLATURE

| | | |
|---|---|---|
| $a$ | - | speed of sound |
| $c$ | - | incompressible specific heat |
| $E$ | - | total system energy |
| $E_B$ | - | bulk modulus of elasticity |
| $F$ | - | flux integrals, Eq. (14) |
| $\bar{\bar{I}}$ | - | idenity tensor |
| $P$ | - | pressure |
| $\bar{q}$ | - | velocity vector |
| $\bar{Q}$ | - | heat transfer |
| $s$ | - | entropy |
| $t$ | - | time |
| $T$ | - | temperature |
| $u,v,w$ | - | x-, y-, z- components of velocity, respectively |
| $U$ | - | conserved variable array, Eq. (14) |
| $V$ | - | volume |
| $\delta$ | - | artificial compressibility |
| $\mu$ | - | viscosity |
| $\nu$ | - | kinematic viscosity |
| $\xi$ | - | allocation parameters, Eq. (16) |
| $\rho$ | - | density |
| $\bar{\bar{\tau}}$ | - | stress tensor |

## INTRODUCTION

Leakage flow through seals in high pressure turbopumps has an important effect on the dynamic behavior of the pumps. The rotation of this fluid reduces the damping forces and generates a subsynchronous whirl instability at a speed of approximately twice the pump critical speed, as first shown by Black (Ref. 1). The Space Shuttle Main Engine (SSME) currently operates near this instability limit. Uprating of the SSME requires an increase in pump speeds, thus additional damping is required. Recently, von Pragenau (Ref. 2) suggested the use of stator roughness to produce turbulent flow in the seal. The flow provides additional damping for the pump, as was demonstrated analytically in Ref. 2. From his work the impetus was provided for numerical and experimental investigations into the damping seals. This paper discusses the numerical modeling of these seals.

A realistic analysis of the flow in the SSME turbopumps requires an unsteady liquid flow solver. Historically, liquid, or incompressible solutions of the Navier-Stokes equations have been steady state. The continuity equation is written as $\bar{\nabla} \cdot \bar{q} = 0$, which implies an infinite sound speed, thus explicit and, consequently, unsteady methods cannot be obtained. This formulation also complicates the calculation of flowfield pressures, which are an important parameter for determining damping forces. The treatment of the velocity-pressure coupling then becomes of paramount importance in developing the numerical model for damping seals. This problem will be discussed further in the next section.

The numerical procedure used in the solution method is based on the **VAST** (**VA**riational **S**olution of the **T**ransport equations) code for compressible flows developed by Prozan (Refs. 3-5). The VAST code is a finite difference analysis which employs a dynamic differencing scheme based on the hypothesis of a variational principle for the governing equations. This formulation promotes the stability of the system and reduces computational requirements. To use the variational approach, the equation governing the velocity-pressure coupling must be considered when deriving the variational equation.

Since turbulent flow is the mechanism which produces the additional damping in the seal, the code must include a turbulence model. There are numerous models to choose from, but again, when transport equation models are considered, the differencing scheme and

the variational equation are affected. Roughness effects must be included in any model, and this aspect can only be handled empirically.

Once developed, the performance of the numerical model must be verified. Results on the damping seals test configuration can then be obtained and the model refined. With the basic model, results using LOX and $LH_2$ (liquid oxygen and liquid hydrogen) can be compared to the analyses of Ref. 2. These cases do not make good verification problems because the properties, and consequently the accuracy of results, of LOX and $LH_2$ are not as well known as other fluids, such as water. The final model developed in the work can be used to perform parametric studies of potential SSME configurations.

## TREATMENT OF THE VELOCITY-PRESSURE COUPLING

The solution of the governing equations in primitive variable form for incompressible flows has proven to be a difficult task. The number of different equation sets used is nearly as large as the number of researchers working in the field. This is in sharp contrast to the solution of compressible gas flow in which, with the ideal gas assumption, the equations are well known. For incompressible and/or liquid flows, there is no comparable equation of state with which to close the system of equations. Density, and consequently pressure, are usually eliminated from the continuity equation, which becomes a constraint on the momentum equations. Although the pressure does appear in the momentum equations as spatial derivatives, neither of these equations can be solved for pressure without introducing directional bias (Ref. 6); nor can a transient type of solution be developed. Thus, from the outset one is faced with "N" equations for "N + 1" unknowns.

Early numerical solutions to incompressible flow avoided this problem by using the vorticity-stream function formulation, which is thoroughly treated in Ref. 6. This procedure suffers from many well known limitations, particularly for internal and three-dimensional problems (see, e.g., Refs. 6,7). With the realistic three-dimensional problems which are within reach by using current and future generations of supercomputers, the use of these equations will be severely limited.

One of the first procedures for obtaining pressures of incompressible flows required the solution of a Poisson equation (Ref. 6). This equation has the form

$$\nabla^2 P = S \qquad (1)$$

where S is a non-linear function of the velocities and their first three derivatives. Also, Neumann boundary conditions are required to solve Eq. (1). The solution to Eq. (1) must be obtained iteratively at each step, a very time consuming process. Another drawback is that the solution does not behave well when complex geometries are being studied. Furthermore, the solution of Eq. (1) only once at each time step does not properly account for the velocity-pressure coupling, as demonstrated in Ref. 8. Since it is well known, Eq. (1) was specifically studied for inclusion into the damping seals model;

however, because of the problems mentioned above, it was determined to be a non-viable alternative.

An increasingly popular solution used in finite difference applications is the artificial compressibility developed by Chorin (Ref. 9). This formulation assumes an equation of state as

$$P = \rho / \delta \tag{2}$$

where $\delta$ is the artificial compressibility. Using Eq. (2) the continuity equation becomes

$$\delta\left(\frac{\partial P}{\partial t}\right) + \bar{\nabla} \cdot \bar{q} = 0 \tag{3}$$

Eq. (3) allows for an explicit finite difference solution for P; however, since $\delta$ is technically a relaxation parameter and has no physical basis, unsteady solutions are meaningless. Steady state solutions, on the other hand, have been obtained successfully by numerous researchers. Chang and Kwak (Ref. 10) and Kwak, et al (Ref. 11) present one the of the most in depth and most successful applications of the method, including applications to SSME problems (Ref. 12).

A Finite Element Method (FEM) which embodies the same general principle as artificial compressibility is the penalty function formuation (Ref. 13). This procedure is widely used in pure FEM techniques, although many variants have been introduced in an attempt to obtain accurate results (for example, Refs. 14, 15). This further serves to illustrate the difficulty of obtaining pressures for incompressible flows.

The artificial compressibility method was considered for use in developing the damping seals model, however, the essentially arbitrary nature of $\delta$ in Eq. (3) creates several problems. Perhaps the major difficulty is in the use of the variational scheme. With no physical basis for $\delta$, the differencing procedure did not behave well. Other problems include the trial and error procedure required to determine $\delta$, and the unavailability of an unsteady solution.

There are numerous other methods for treating the velocity-pressure coupling, such as the transformed equations of Solomon and Szymczak (Ref. 16) or the assumed elemental "deviatoric stress-velocity-pressure" method of Yang and Atluri (Ref. 17). Few of these methods provide a set of physically accurate equations for the primitive variables. Also, transient problems can, at best, only be "studied" by iterating for successive steady state solutions, which is very costly and inefficient. Numerical damping is also necessary to obtain solutions in most of the available methods, including the artificial compressibility method.

A recently developed procedure which attempts to overcome most of these deficiencies is presented in Ref. 18. This work develops the pressure solution based on a finite sound speed, in other words, a compressible formulation. The compressibility is used to obtain an equation of state, which in turn introduces the pressure into the compressible form of the continuity equation. The resulting equation is

$$\left(\frac{\partial P}{\partial t}\right) + \bar{q} \cdot \bar{\nabla} P + \rho c^2 \, (\bar{\nabla} \cdot \bar{q}) = 0 \qquad (4)$$

Eq. (4) has been successfully applied in Ref. 18 to both transient and high Reynolds number problems.

The procedure to be used in developing the damping seals model is very similar to that of Ref. 18. The final equation differs somewhat from Eq. (4) because fewer assumptions will be made. The details of the analysis will be presented in the next section.

## THEORY

### Basic Equations

In the development of the compressible VAST code, the integral form of the equations of motion are used. Several advantages of this formulation occur, as pointed out in Ref. 5. The fundamental equations are:

continuity:

$$\iiint_{cv} \frac{\partial \rho}{\partial t} dV + \iint_{cs} \rho \bar{q} \cdot d\bar{s} = 0 \qquad (5)$$

momentum:

$$\iiint_{cv} \frac{\partial \rho \bar{q}}{\partial t} dV + \iint_{cs} [(\rho \bar{q})\bar{q} + (\bar{\bar{I}}P - \bar{\bar{\tau}})] \cdot d\bar{s} = \bar{0} \qquad (6)$$

energy:

$$\iiint_{cv} \frac{\partial \rho E}{\partial t} dV + \iint_{cs} [\rho E \bar{q} + (\bar{\bar{I}}P - \bar{\bar{\tau}}) \cdot \bar{q} + \bar{Q}] \cdot d\bar{s} = 0 \qquad (7)$$

For this analysis, as with all incompressible methods, the assumption is made that $P \neq P(T)$, hence the energy equation (Eq. 7) decouples from the other equations. The equation is listed here since, if heat transfer or thermal data were desired, Eq. (7) could be solved independently for temperature. This equation will not be used in the remainder of the analysis as only isothermal problems will be considered. Since liquid flows are to be studied, it should also be pointed out that gravity, if assumed to be important, is easily included in Eq. (6) as a source term.

Pressure Solution

As previously discussed, the current approach to the pressure solution is to take advantage of the finite sound speed in all fluids, liquid or gas. The procedure is more correctly called a slight compressibility method, rather than an incompressible method.

An equation of state is assumed to exist in the form

$$P = P(\rho) \tag{8}$$

The compressiblity of any fluid is expressed by the bulk modulus of elasticity,

$$E_B = \frac{dP}{\frac{d\rho}{\rho}} \tag{9}$$

and the finite acoustic speed in a liquid is given by

$$a^2 = \frac{E_B}{\rho} = \frac{dP}{d\rho} \tag{10}$$

The equation of state may now be written as

$$dP = a^2 d\rho \tag{11}$$

To derive the pressure equation, Eq. (11) is primarily used in differential form, however, a reference state must also be assumed for integration purposes. This reference state, $P_r$ and $\rho_r$, must be assumed to be the usual theoretical incompressible values of P and $\rho$ for the fluid being considered. Substitution of Eq. (11) into Eq. (5) now yields the pressure equation.

$$\iiint_{cv} \frac{\partial P}{\partial t}\, dV + \iint_{cs} P\bar{q}\cdot d\bar{s} + (\rho_r a^2 - P_r) \iint_{cs} \bar{q}\cdot d\bar{s} = 0 \qquad (12)$$

The convective part of Eq. (12) is written as two terms to facilitate discussion of some salient features of the method. First, it should be noted that as the sound speed, a , approaches infinity (the true incompressible case) Eq. (12) reduces to the standard incompressible form of continuity. Another feature is that the artificial compressibility method can be viewed as a limiting case of Eq. (12). If the contribution of the pressure to the convective terms is discarded and $\rho_r a^2 = 1/\delta$, then Eq. (12) reduces to the integral form of Eq. (3). Perhaps the most important feature is the physical reasoning used to obtain Eq. (12). In addition to more correctly describing the physics of the flowfield, this method allows the use of a variationally based dynamic differencing scheme.

Eq. (11) could, and perhaps should also be included in the momentum equations. The error introduced by using $\rho = \rho_r$ in Eq. (6) is essentially zero for steady state solutions, which can be viewed as incompressible solutions. For unsteady solutions, the error is of order $\Delta P/\rho a^2$ vs. $\rho$ and, since a is large, this error is assumed to be negligible.

Numerical Analog

The numerical integration used to solve Eqs. (6) and (12) is based in part on the variational procedure developed by Prozan in Refs. 3-5. This procedure will be summarized below, and the application to the current work will then be discussed.

The compressible VAST transport equations may be generalized as

$$\frac{\partial}{\partial t} \iiint_{cv} U_n\, dV = -F_n \quad ; \quad n = 1,\ldots,5 \qquad (13)$$

where

$$U = \begin{Bmatrix} \rho \\ \rho\bar{q} \\ \rho E \end{Bmatrix} \quad ; \quad F = \iint_{cs} \begin{Bmatrix} \rho\bar{q}\cdot d\bar{s} \\ [\rho\bar{q}\bar{q} + (\bar{\bar{I}}P - \bar{\bar{\tau}})]\cdot d\bar{s} \\ [\rho E\bar{q} + (\bar{\bar{I}}P - \bar{\bar{\tau}})\cdot\bar{q} + \bar{Q}]\cdot d\bar{s} \end{Bmatrix} \qquad (14)$$

Now, the domain of integration is subdivided into E finite elements and Eqs. (13) become

$$\sum_{e=1}^{E} (\Delta U_n \ \Delta V/\Delta t)_e = - \sum_{e=1}^{E} F_{n,e} \qquad (15)$$

A functional distribution of the variables is assumed over the surfaces of the elements and the flux terms $F_{n,e}$ are evaluated using values from the previous time step.

The $(\Delta U_n \ \Delta V/\Delta t)_e$ represent the total accumulation of the nth conserved quantity within element e. To obtain the conserved variables at a new time step, nodes are placed at the corners of each element and the $(\Delta U_n \ \Delta V/\Delta t)_e$ are allocated to the various nodes. Thus, the conserved quantities at the nodes are determined by assembling the contributions from its surrounding elements. This accumulation can be written

$$(\Delta U_n \ \Delta V/\Delta t)_j = - \sum_{e=1}^{k} \xi_{n,e,j} \ F_{n,e} \qquad (16)$$

where j is the node number, k is the total number of elements surrounding node j, and the $\xi_{n,e,j}$ are the allocation parameters.

The assembled equation, Eq. (16) is analogous to a finite difference expression in which the spatial transformations are numerically embedded in the analog. It may be interpreted as a general form of the finite difference scheme since different finite difference algorithms can be derived with selected allocation parameters. The VAST differencing procedure differs from other schemes in that it does not dictate a fixed $\xi_{n,e,j}$ throughout the course of integration, but rather, changes the parameters dynamically in both time and space according to the variational principle. This principle requires that the rate of entropy production be maximized. The VAST differencing scheme thus uses the transport equations as equality constraints and dynamically determines the allocation parameters to achieve maximum stability of the system.

To apply the VAST numerical analog to the current investigation, a procedure for determining the allocation parameters similar to the procedure of the Ref. 5 must be developed. A first attempt of this development was presented in Ref. 19. This method was not entirely satisfactory, and further research was performed. The entropy

functional of Ref. 19 was further manipulated and the following derivatives were obtained:

$$\frac{\partial \rho s}{\partial P} = \left[\frac{1}{a^2} \quad c \ln T - c + \frac{1}{2}\frac{q^2}{T}\right] \tag{17}$$

where c is the specific heat,

$$\frac{\partial \rho s}{\partial \rho u} = -\frac{u}{T} \tag{18a}$$

$$\frac{\partial \rho s}{\partial \rho v} = -\frac{v}{T} \tag{18b}$$

$$\frac{\partial \rho s}{\partial \rho w} = -\frac{w}{T} \tag{18c}$$

Using Eqs. (17) and (18), the allocation parameters of Eq. (16) are determined in the same manner presented in Ref. 5. This procedure provided good stability for many cases, however, some problems were encountered with the pressure equation. Eventually, a centered difference scheme was used for the pressure equation for all time and all nodes while continuing to use Eqs. (18) for the momentum equations. This method has, thus far, produced satisfactory results on all the problems attempted, although some damping of Eq. (12) is necessary.

## Turbulence Model

To accurately model the damping seals problem, a turbulence model must be included in the code. Turbulent flow is an important parameter in the performance of the damping seals, and roughness is used to produce this flow. Hence, the model must ultimately include roughness effects. All turbulence models in current use have a considerable amount of empiricism included. Even the more advanced Reynolds stress transport equations require several empirical constants for closure. Roughness effects in any model are, at best, accounted for by these empirical constants, thus it was decided to use an algebraic model in the code development.

To develop a turbulence model for use in the VAST codes, special wall element functions were developed to avoid using an excessive number of grid points near the wall. This model was discussed in Ref. 19, but will be included here for completeness. For smooth walls and fully developed pipe flow, the following empirical logarithmic profiles are valid.

$$u^+ = y^+ \quad , \; y^+ < 5 \tag{19a}$$

$$u^+ = -3.05 + 5.0 \ln(y^+), \; 5 \le y^+ \le 30 \tag{19b}$$

$$u^+ = 5.5 + 2.5 \ln(y^+) \quad , \; y^+ > 30 \tag{19c}$$

where

$$u^+ = u / u^*$$

$$u^* = \sqrt{\tau_w / \rho}$$

$$y^+ = u^* y / \nu$$

and y is the distance from the wall. From Eq. (19a), the velocity gradient at the wall is

$$\left(\frac{\partial u}{\partial y}\right)_w = (u^*)^2 / \nu \tag{20}$$

In terms of real distance from the wall, Eq. (19c) represents most of the boundary layer, therefore the following computational procedure is employed. A fictitous wall is assumed to be 0.0005 feet (approximately $y^+ = 30$) away from the real wall and it is assumed that no flow occurs between these two walls ($\dot{m}=0$) . If a slip boundary condition is used, u is determined from the momentum equations, and $u^*$ at 0.0005 feet is determined from Eq. (19c). Since this equation is not explicit in $u^*$, an empirical approximation is made:

$$u^* = 0.1662529 \; u^{0.867325} / \; (y/\nu)^{0.132675} \tag{21}$$

Eqs. (20) and (21) now give the velocity gradient and shear stress at the wall. An eddy viscosity is used to determine both the local shear stress and the variation of this stress with distance from the wall, y.

$$\mu_T = 0.07\, u^* \rho r \ell + \mu \qquad (22)$$

where r is the radius for pipe flows, and

$$\ell = (y/.3r) \quad , \quad 0 < (y/r) < .3$$
$$\ell = 1.0 \quad , \quad (y/r) \geq .3$$

To include roughness in the turbulence model outlined above, the empircal constants of Eqs. (19) - (22) must be changed accordingly. Ref. 20 presents the information necessary for these changes.

## RESULTS

In order to verify the performance of the model during development, several simple two-dimensional test cases were run. Results from these problems were presented in Ref. 19. Those results were obtained on the Continuum CM-1000 workstation (Intel 8086 microprocessor). One important conclusion that came from the early runs was the long run times associated with the CFL constraint. These run times coupled with the geometric necessity to use a large number of grid points to model damping seals, dictated a shift in the development effort to a mainframe computer.

### Vectorization

The computer code was installed on a CRAY-1S vector processor and extended to handle three-dimensional geometries. In order to take advantage of the available computing power, this version of the code was vectorized. The vector FORTRAN used is identical to the language to be used on the MSFC CRAY X-MP. This will allow for installation and efficient operation of the code at NASA MSFC. Once the mainframe programming was completed the two-dimensional problems presented in Ref. 18 were repeated. Results from the mainframe code were in agreement with the previous results, thus other problems with similarities to the damping seals geometry were attempted in order to refine the model.

### Rotating Cylinders

Several cases involving two concentric rotating cylinders were studied. This two-dimensional flow is the Couette flow described in Ref. 2 for the damping seals. Both the differencing scheme and boundary conditions for use in the liquid code were examined using this configuration. This study led to the decision to use Eq. (18) with a centered scheme for pressure in the differencing algorithm. The boundary conditions used on the moving wall were a no-slip condition with a table lookup algorithm to maintain a constant rotational velocity at the wall. The boundary condition must be modified to allow a slip wall when the turbulence model is used, however, the two-dimensional results were obtained for a laminar viscosity.

Velocity vectors for a 10° slice of the cylinders are shown in Figs. 1 and 2 for both air and water as fluids. The surface velocity of the inner cylinder is 200 ft/sec while the

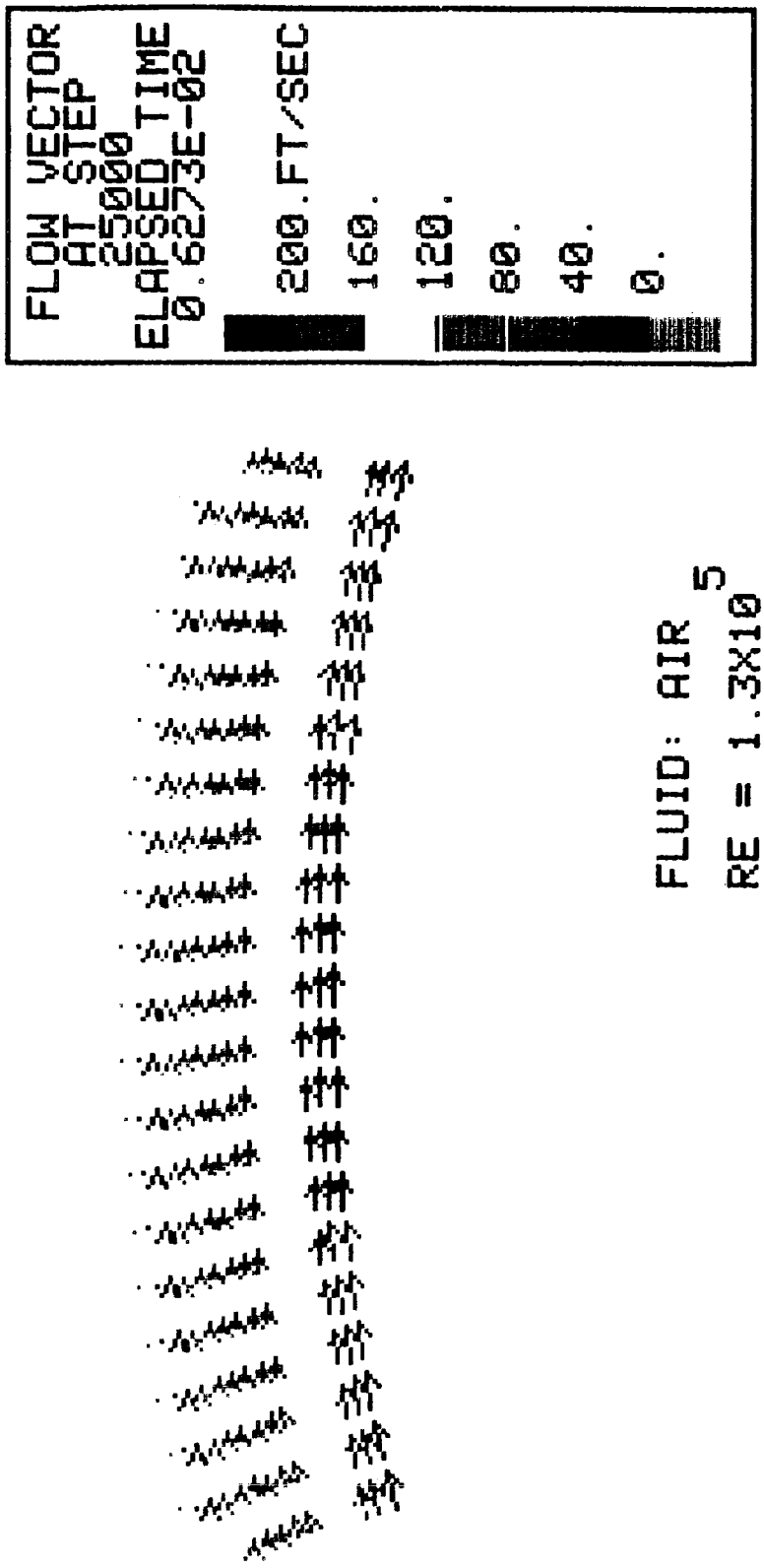


Fig. 1. Couette Flow Velocities for Air.

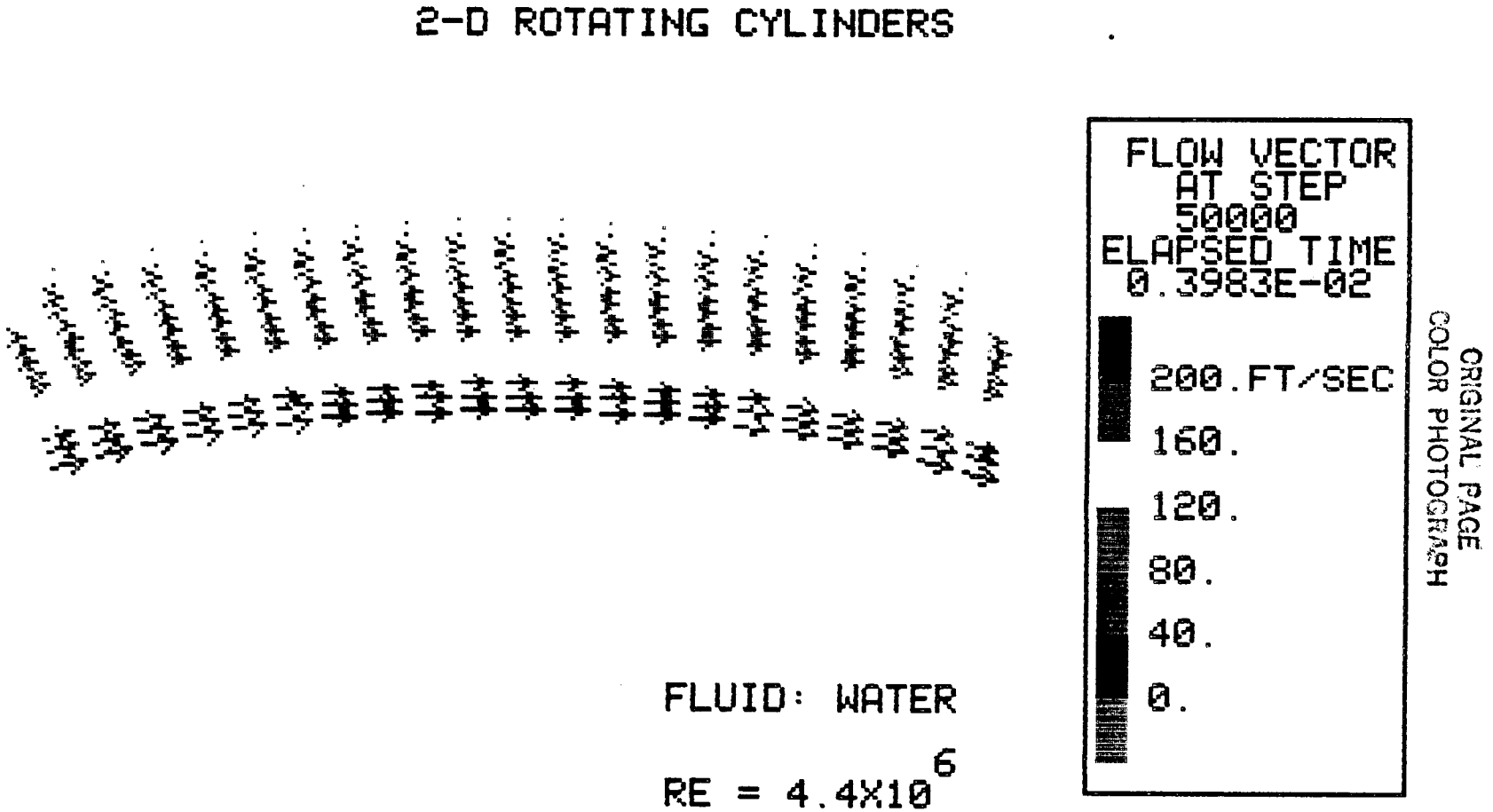


Fig. 2. Couette Flow Velocities for Water.

outer cylinder is stationary. These results are compared to the exact solution in Fig. 3. The agreement is seen to be quite good. The Reynolds numbers of these problems were of order $10^5$ (air) and $10^6$ (water). This range is two to three orders of magnitude higher than any problems attempted by the majority of existing incompressible codes. One reason these large Reynolds numbers can be studied is that the integral formulation, Eqs. (5-7), (12), eliminates cell Reynolds number problems.

The cylinder problem was also run using the compressible VAST code for comparison purposes. These results are also shown in Fig. 3. They do not agree as well with the exact solution. This disagreement can be traced to the behavior of the pressure solution. The initial condition for this problem assumed a constant pressure of 2116 psf. The pressure after 44,000 iterations is shown in Fig. 4. (For the exact solution, the outer cylinder pressure is 2119.33 psf). The constant initial condition caused waves to be generated in the flowfield. These waves were observed to "bounce" back and forth between the cylinders. The no-slip walls are non-porous to these waves, and the absolutely conservative nature of the numerical analog (Ref. 5) coupled with the absence of explicit artificial viscosity do not allow the waves to damp out in this closed system other than through real viscous dissipation. This was verified by running the same problem with the exact solution as an initial condition. No waves were generated, and the pressure essentially did not vary from the exact solution.

Similar pressure waves can be observed in the incompressible code. This is clearly illustrated by the two waves seen in Fig. 5 for the cylinder problem with water. This result together with the velocities (Fig. 3) tends to support the contention that the pressure does not greatly affect the velocity solution for essentially incompressible flows. This idea is important to solution procedures which eliminate the pressure entirely (for example the vorticity-stream function formulation) or decouple the pressure from the momentum equations. This small dependence is also important to the performance of the artificial compressibility method, as the pressures computed during the relaxation are entirely unrealistic. In contrast, Fig. 3 illustrates that compressible solutions, even at very low speeds, are sensitive to pressure effects.

In an attempt to reduce the propagation of pressure waves in a closed system, wall boundary conditions were examined which would allow these waves to pass through, such as occurs at inlets for an open system. This effort was not entirely successful, thus some damping is used in the pressure differencing algorithm.

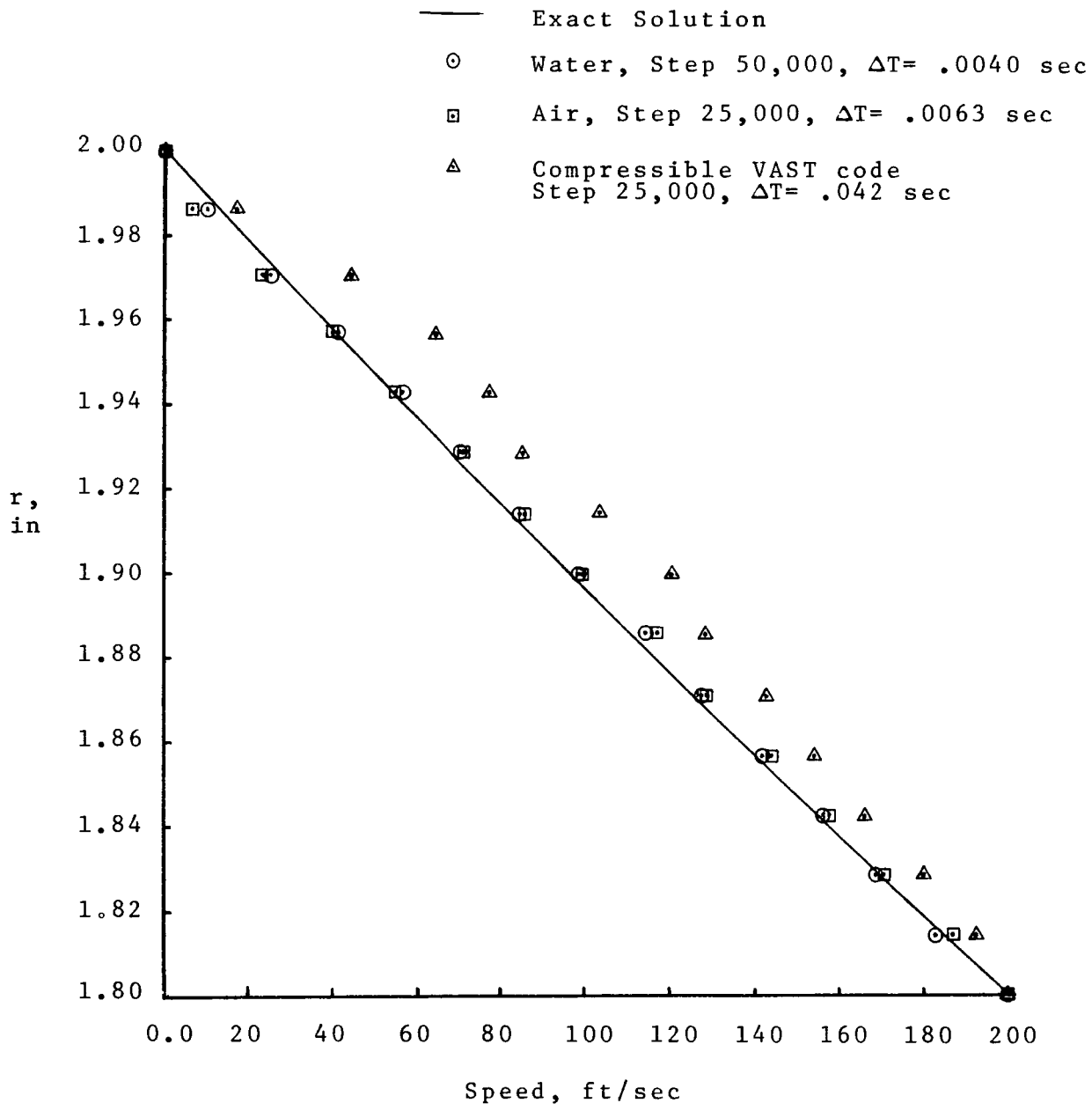


Fig. 3. Radial Velocity Profile for Rotating Cylinders.

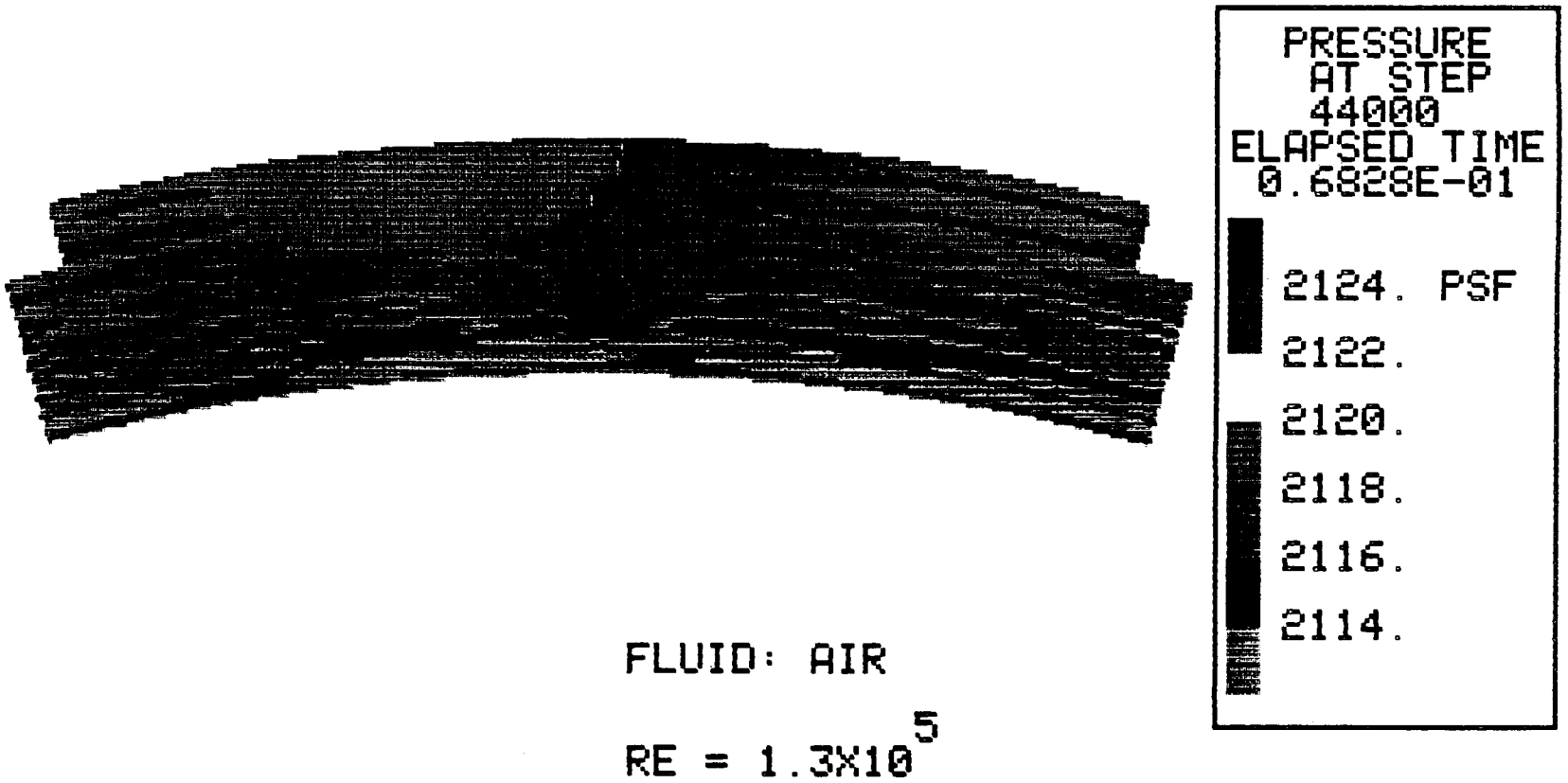


Fig. 4. Pressures for Cylinders with Air from Compressible VAST Code.





ORIGINAL PAGE
COLOR PHOTOGRAPH

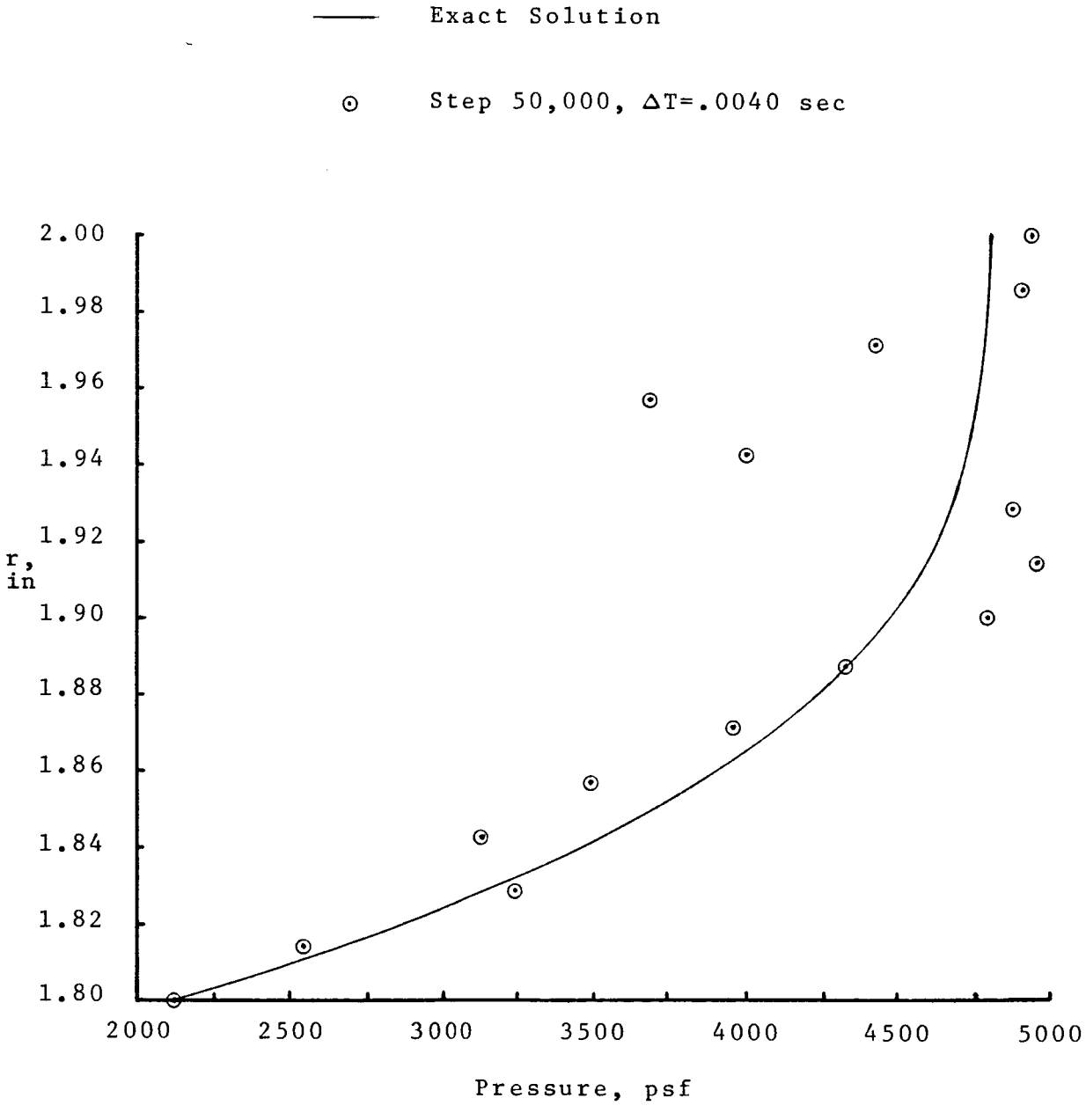


Fig. 5. Radial Pressure Profile for Rotating Cylinders with Water.

The cylinder results shown in Figs. 1 - 5 were obtained using a mesh of 15 x 241 (radial x circumferential) nodes. Thus, an element side is 1.5° of arc in length. To determine the effect of mesh size, the same configuration (with air as the fluid) was repeated using a 15 x 91 mesh, or 4° length of each element. This solution showed poor agreement with the exact solution, proving that good circumferential resolution is required at least when the flow is circumferential in nature.

Three-Dimensional Results

After refining the model based on the two-dimensional rotating cylinder studies, a three-dimensional damping seals configuration was modeled and preliminary results obtained. The grid for the seal, based on the test configuration to be run, is shown in Fig. 6. The gap between the cylinders in magnified in this drawing; actual dimensions are 0.02 inch gap, 1.8 inch rotor diameter and 1.8 inch axial length. The grid resolution is 11x105x26, radial, circumferential and axial, respectively, for a total of 30,030 nodes. This resolution produces typical element length ratios illustrated in Fig. 6. This element shape in conjunction with the two-dimensional mesh study, immediately suggest that more nodes should be used. However, available computer storage on the CRAY-1S will allow 31,000 nodes maximum for this problem. Expanded inlets and outlets to the seal should also be included in an in-depth study, but again, this requires additional nodes. This node limitation will be alleviated by use of the MSFC CRAY X-MP, which will have more than twice the storage available on the CRAY-1S used in this study. It should be pointed out that the large number of nodes required is as much of a physical geometry requirement, as it is a numerical requirement.

The fluid in the three-dimensional study is water ( $\rho_r$=1.89936 slugs/ft$^3$, $P_r$=2116 psf) at 614° R, and the turbulence model was used. The upstream axial boundary condition was a fixed inlet with the velocity profiles (both axial and radial) based on a 1/7 power law profile. The downstream axial boundary condition is a constant integrated mass flow in the axial direction. The rotor speed is 345.6 ft/sec and the axial static pressure drop through the seal is 2000 psi.

Preliminary results for this problem are shown in Figs. 7-9. This is at an early iteration step, not at a steady state. Further results have not been obtained due to needed problem refinement that can only be provided by the CRAY X-MP. Furthermore,

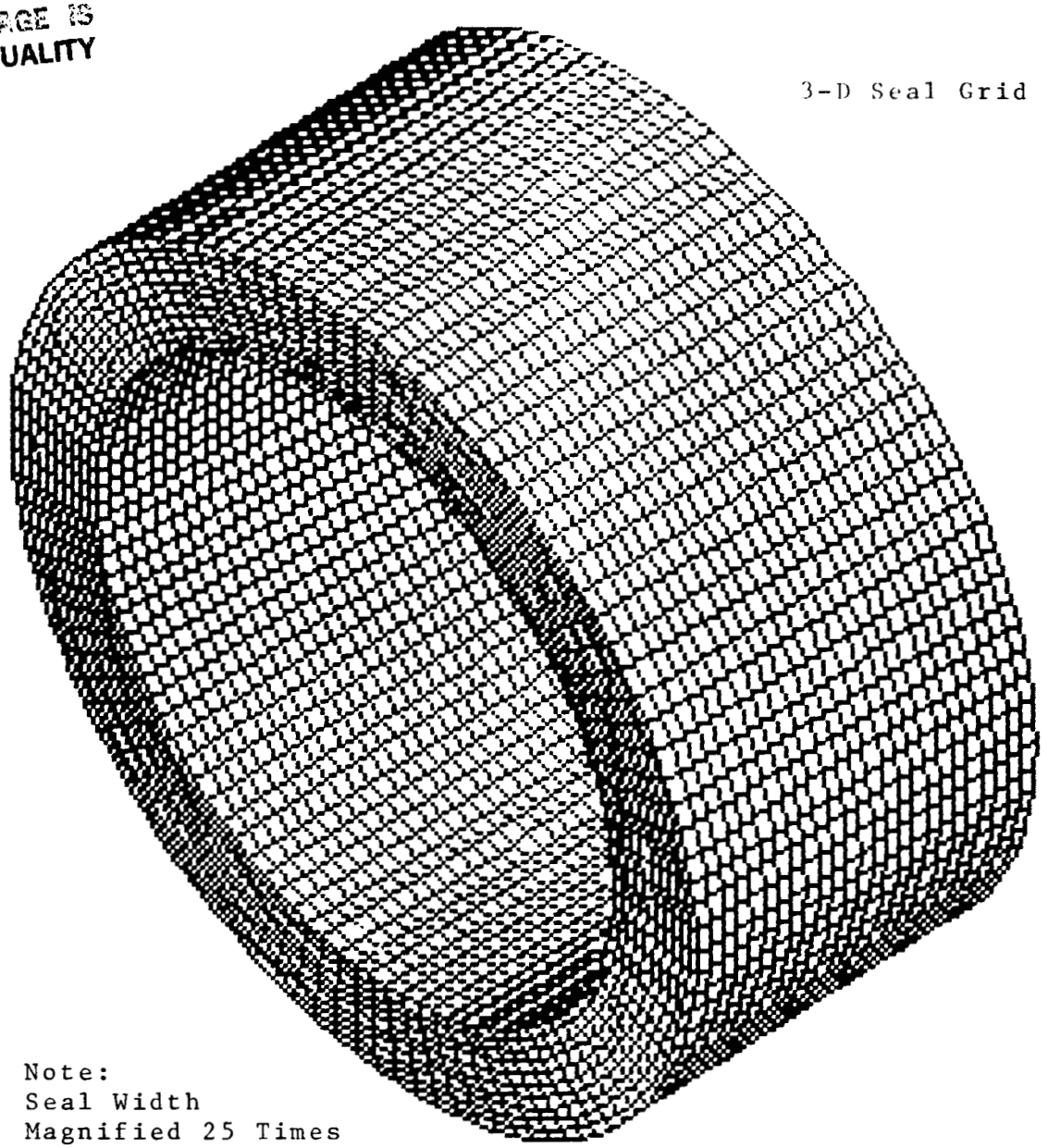


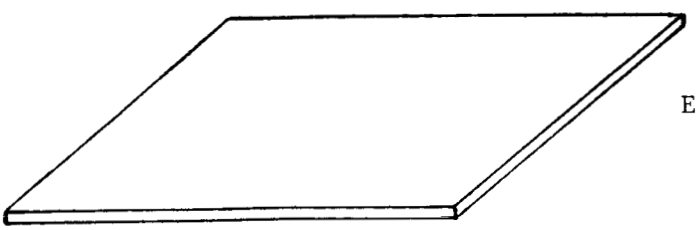


Fig. 6. Grid and Element Detail for Damping Seal Model.

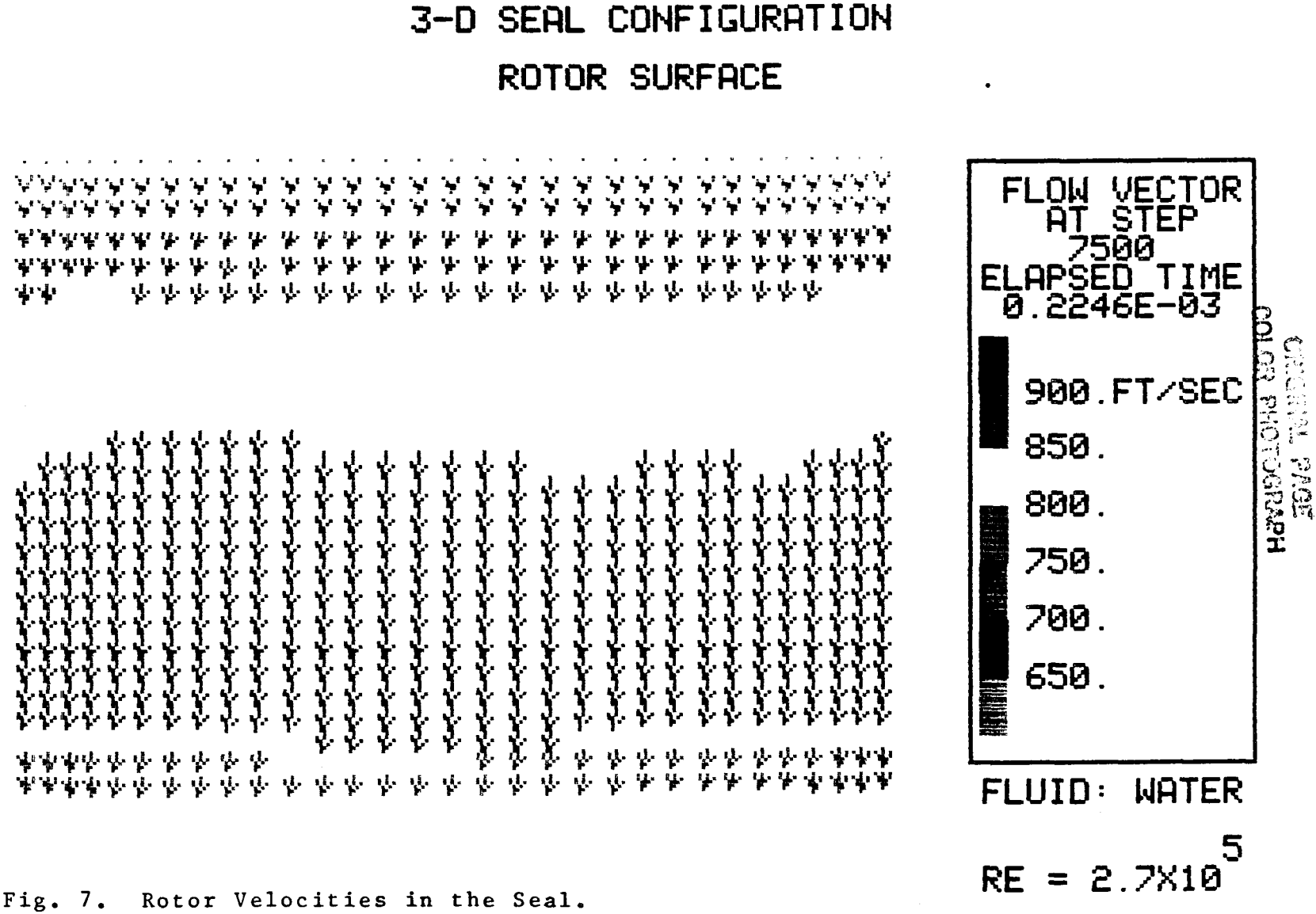


Fig. 7. Rotor Velocities in the Seal.

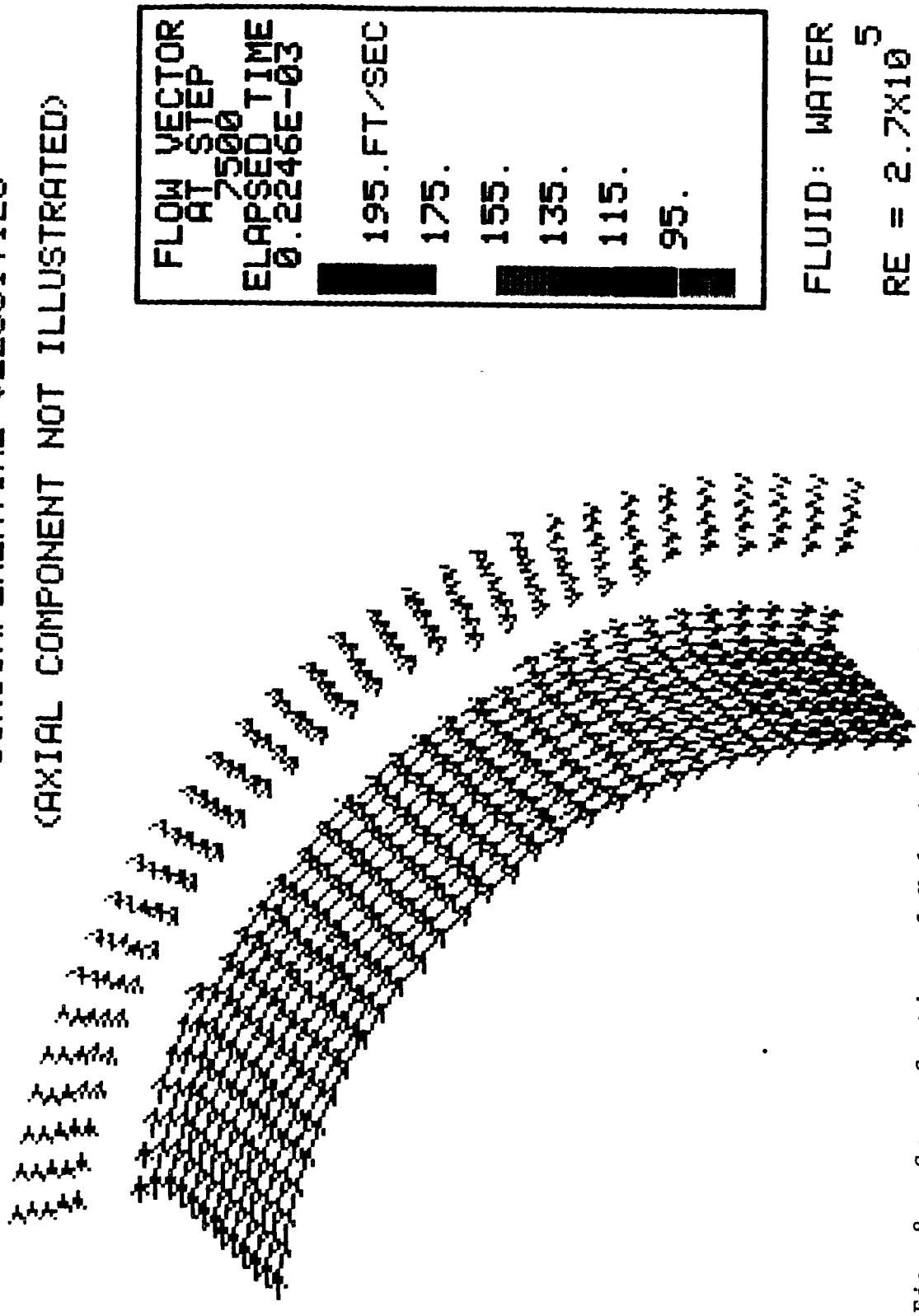


Fig. 8. Cross-Section of Velocities in the Seal.

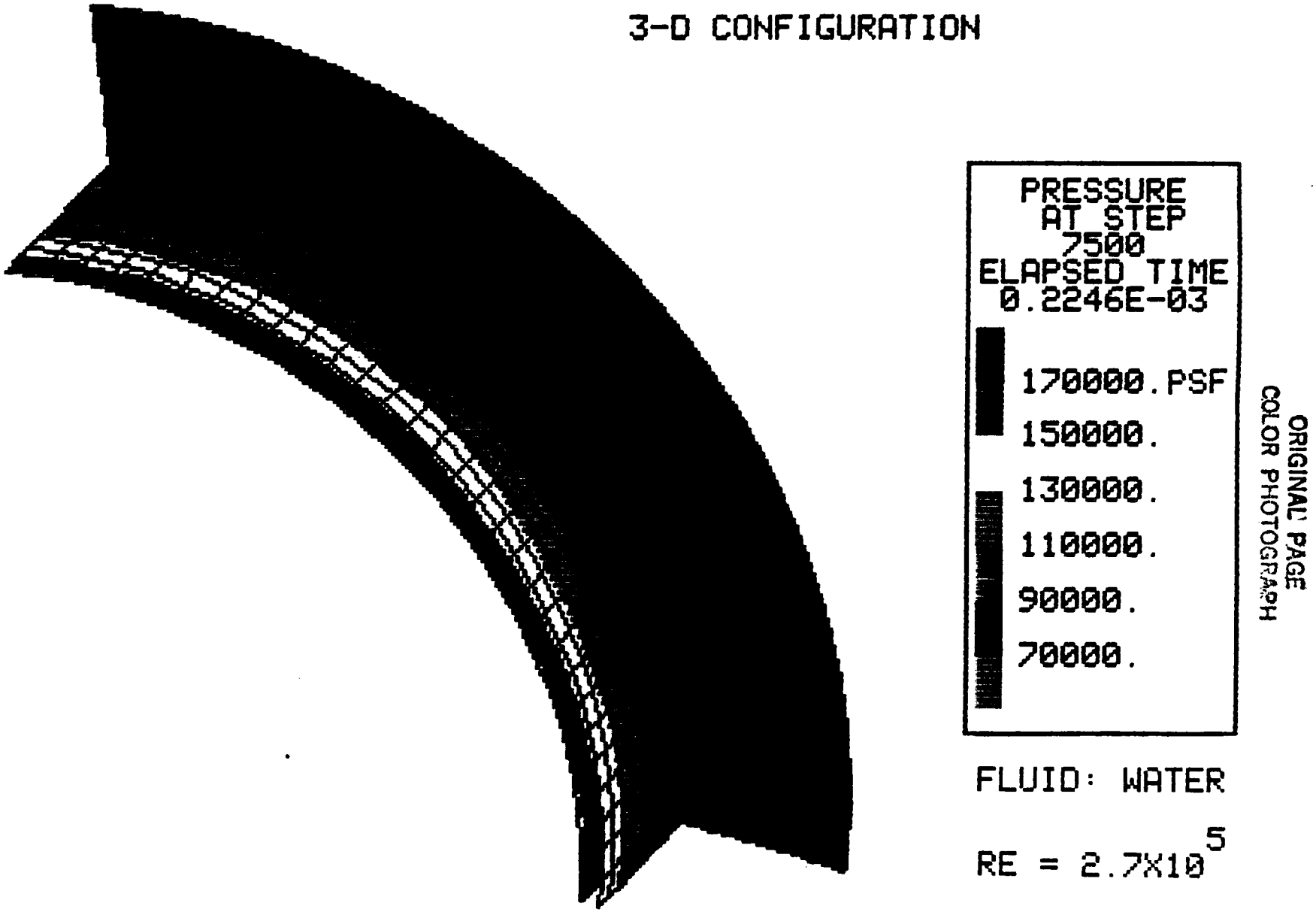


Fig. 9. Cross-Section of Pressures in the Seal.

experimental data is not yet available for comparisons. Fig. 7 shows the velocity vectors on the rotor surface for a 105° slice which has been "unrolled". The initial condition was the 345.6 ft/sec speed circumferentially, with 0.0 ft/sec axial flow at the wall. The development of the axial flow based on the "slip condition" in the turbulence model is seen to be quite good. Since the upstream inlet (top of figure) is held at zero axial velocity although there is a circumferential component (which does not show on the scale used), the flow must develop along the length of the rotor. This development is also proceeding well. This result suggests that, to get the proper characteristics in the seal, the upstream boundary condition should be changed, or else some type of inlet extension should be included, preferably the latter choice to more correctly model the test configuration.

Studying the circumferential direction at a fixed axial location in Fig. 7, some unexpected variations in the velocity vectors are seen. An examination of the full 360° data shows that this pattern repeats at exactly 90° intervals. This suggests a dependence on the grid resolution and the element shape, as discussed on the two-dimensional problem, and seen in Fig. 6.

At an axial station in the fully developed flow region of Fig. 7 (at approximately 75 % of the seal length) velocities and pressures are plotted in Figs. 8 and 9, respectively. The axial component of the velocity is not illustrated in Fig. 8. Once again, the velocities at the walls are seen to be different from the cylinder velocities. This is expected due to the turbulence model, since this is actually the velocity at $y^+ = 30$ away from the walls. The turbulent profile is seen here to be developing quite well. Figure 9 shows the pressures at the same surfaces. The pressures are behaving well, with no large waves propagating at this location.

## Computational Requirements

From the two- and three-dimensional results just discussed, mainframe computer requirements can be established for the code. As previously mentioned, storage requirements are large and indeed, the limit of 31,000 nodes for three-dimensional, turbulent problems is too small. Considerably larger numbers of nodes can be used for three-dimensional laminar, or any two-dimensional problems. This nodal limit will more than double on a CRAY X-MP. CPU times for a CRAY-1S computer have been established as follows:

two-dimensional, viscous, laminar problems, $1.8 \times 10^{-5}$ sec/node/step
three-dimensional, viscous, turbulent problems, $8.9 \times 10^{-5}$ sec/node/step

These times will be approximately a factor of 10 faster on a CRAY X-MP. Comparison of these resource requirements with other CFD codes show that they are very similar, and perhaps even smaller than existing methods (see for example Ref. 12).

## CONCLUSIONS

One of the principle objectives of the research work reported herein was to produce a high Reynolds number, explicit CFD code for liquid and/or incompressible flow regimes. Considerable effort was expended on this task with good results. The code which has been developed has been applied to several problems, with results comparable to any existing code, including the much studied artificial compressibility codes. Computer requirements necessary to generate solutions is also comparable to or less than requirements of other codes. However, flow problems at much higher Reynolds numbers than exist in the majority of the literature have been presented. There is much room for improvement in the model to further increase its utility. In particular, the proper accounting for pressure in the variational approach, and consequently the differencing scheme, would enhance the stability and overall performance of the method.

Two-dimensional problems similar in character to the damping seals have been studied, and the computer model refined based on these results. Preliminary studies of a three-dimensional seal model have also been made. However, several comparisons with other seal analyses have not been made. In particular, the anticipated experimental data which is important to the model verification has not become available during the course of this study. Liquid oxygen and liquid hydrogen studies(which are presented in the bulk flow analysis of Ref. 2) are not good problems for use in model refinement due to the extreme physical characteristics of the fluids. Such refinement should be made prior to performing parametric studies because of the large amount of computer resources necessary to perform these studies.

To improve the efficiency of the computer code, so that the experimental and parametric studies can be performed once the data becomes available, the code has been vectorized and developed to run on the CRAY X-MP to be installed at MSFC. This will also help provide NASA in-house capabilities to model turbomachinery.

## REFERENCES


1. Black, H.F., "Effects of Hydraulic Forces in Annular Pressure Seals on the Vibrations of Centrifugal Pump Rotors," J. Mechanical Engineering Science, Vol. 11, No. 2, 1969.

2. von Pragenau, G.L., "Damping Seals for Turbomachinery," NASA TP 1987, 1982.

3. Prozan, R.J., "A Variational Principle for Compressible Fluid Mechanics, Discussion of the One-Dimensional Theory, " NASA CR-3526, April 1982.

4. Prozan, R.J., "A Variational Principle for Compressible Fluid Mechanics, Discussion of the Multi-Dimensional Theory," NASA CR-3614, October 1982.

5. Prozan, R.J., "Hypothesis of a Variational Principle for Compressible Fluid Mechanics," CI-TR-0086, 1985.

6. Roache, P.J., Computational Fluid Mechanics, Hermosa Publishers, Albuquerque, N.M., 1982.

7. Gunzburger, M.D. and J.S. Peterson, "On the Finite Element Approximation of the Stream Function - Vorticity Equations," Advances in Computer Methods for Partial Differential Equations V, R. Vichnevetsky and R.S. Stepleman (eds.), IMACS, pp. 47-56, 1984.

8. Raithby, G.D. and G.E. Schneider, "Numerical Solution of Problems in Incompressible Fluid Flow: Treatment of the Velocity-Pressure Coupling," Num. Heat Transfer , Vol 2, pp. 417-440, 1979.

9. Chorin, A.J., "A Numerical Method for Solving Incompressible Viscous Flow Problems," J. of Computational Physics, Vol. 2, pp. 12-26, 1967.

10. Chang, J.L.C. and D. Kwak, "On the Method of Pseudo Compressibility for Numerically Solving Incompressible Flows," AIAA Paper 84- 252, January 1984.

11. Kwak, D., J.L.C. Chang, S.P. Shanks, and S. Chakravarthy, "A Three-Dimensional Incompressible Navier-Stokes Flow Solver Using Primitive Variables," AIAA J., Vol 24, No. 3, 1986.

12. Kwak, D., "Viscous Incompressible Flow Computation - A Summary of Recent Progress at Ames," SSME Computational Fluid Dynamics Fourth Working Group Meeting. Marshall Space Flight Center, AL, April 1986.

13. Hughes, T.J.R., W.K. Liu, and A. Brooks, "Finite Element Analysis of Incompressible Viscous Flows by the Penalty Function Formulation," J. of Computational Physics, Vol. 30, 1979, pp. 1-60.

14. Engleman, M.S., R.L. Sani, P.M. Gresho, and M. Bercovier,"Consistent vs. Reduced Integration Penalty Methods for Incompressible Media Using Several Old and New Elements," Int. J. Numerical Methods in Fluids, Vol 2, pp. 25-42, 1982.

15. Kheshgi, H.S., and L.E. Scriven, "Variable Penalty Method for Finite Element Analysis of Incompressible Flow," Int. J. for Numerical Methods in Fluids, Vol 5, pp. 785-803, 1985.

16. Solomon, J.M. and W.G. Szymczak, "Finite Difference Solutions for the Incompressible Navier-Stokes Equations Using Galerkin Techniques," Fifth IMACS International Symposium on Computer Methods for Partial Differential Equations, Lehigh Univ., PA., June 1984.

17. Yang, C. and S.N. Atluri, "An Assumed Deviatoric Stress-Velocity-pressure Mixed Finite Element Method for Unsteady, Convective, Incompressible Viscous Flow: Part I: Theoretical Development," Int. J. for Numerical Methods in Fluids, Vol 3, pp. 377-398, 1983.

18. Kawahara, M. and Hirano, H.,"A Finite Element Method for High Reynolds Number Viscous Fluid Flow Using Two Step Explicit Scheme," Int. J. for Numerical Methods in Fluids, vol. 3, pp. 137-163, 1983.

19. Abernathy, J.M., and R. C. Farmer,"Computational Fluid Mechanics Utilizing the Variational Principle of Modelling Damping Seals," Interim Report, Contract NAS8-35508, NASA Marshall Space Flight Center, AL., 1985.

20. Schlichting, H., Boundary Layer Theory, 6th ed., McGraw Hill, New York, 1968, pp. 578-589.